Available online at www.sciencedirect.com
ScienceDirect
Journal of Crystal Growth 307 (2007) 192–202
JOURNAL OF CRYSTAL GROWTH
www.elsevier.com/locate/jcrysgro

Phase behaviour in binary mixed Langmuir–Blodgett monolayers of triglycerides

Aneliya N. Zdravkova, J.P.J.M. van der Eerden*

Department of Condensed Matter and Interfaces, Utrecht University, P.O. Box 80000, 3508 TA, Utrecht, The Netherlands

Received 29 January 2007; received in revised form 25 May 2007; accepted 30 May 2007
Communicated by Y. Furukawa
Available online 2 June 2007

Abstract

Binary mixed monolayers of the triglycerides (TAGs)-tripalmitin (PPP), tristearin (SSS) and triarachidin (AAA) at the air–water interface are investigated with the Langmuir method. Langmuir–Blodgett (LB) layers obtained by deposition on mica are investigated by Atomic Force Microscopy. Combining Langmuir and AFM results the relation between the phase behaviour of binary mixed TAGs and their chain length is established. TAG mixtures form monolayers with molecules in trident conformation at the air–water interface, like pure TAGs. The area $A_{cond} = 63\,\text{Å}^2$ and the pressure $\pi_{cond} = 8$–$10\,\text{mN/m}$ that separate "gas" and "condensed" film structures are the same for all mixtures and pure systems. In the $\pi-A$ isotherms the sharpness of the transition from "gas" to "condensed" phase decreases with the average chain length for all systems. Using AFM data the monolayer thicknesses for mixtures and pure systems is found to be linearly dependent on the average chain length of the TAG molecules. A linear relation between film thickness and applied AFM force is established. The corresponding coefficient $\tilde{K}$ is higher for mixed monolayers ($\tilde{K} = 0.08 \pm 0.01\,\text{nN}^{-1}$) than for pure systems ($\tilde{K} = 0.07 \pm 0.01\,\text{nN}^{-1}$). AFM images show phase separation in the systems PPP–SSS and PPP–AAA. The solubility of the shorter PPP molecules in the "long" (SSS- and AAA-rich) phase is significant. For the mixture SSS–AAA, phase separation is not observed. In that mixture the monolayer thickness varies linearly with composition, supporting the conclusion that SSS and AAA mix almost ideally. The main driving force for phase separation is the difference in the alkyl chain length. Indeed PPP–AAA (length difference 4 C atoms) shows the most clear phase separation. The relatively weak phase separation in PPP–SSS and the absence of phase separation in SSS–AAA show that the influence of chain length difference decreases with increasing average chain length. In air PPP–SSS and PPP–AAA mixed monolayers are unstable and crystals with α- and β-like structure are formed on top of the monolayer as in pure PPP and SSS systems.

PACS: 68.18; 68.37.Ps; 68.47.Pe

Keywords: A1. Atomic force microscopy; A1. Langmuir–Blodgett technique; A1. Surface structure; B1. Triglycerides

1. Introduction

Because triglycerides (TAGs) are the main components in natural fats, they have been studied for many years. Most of the research focused on the melting and crystallization properties of TAGs. An overview of the thermodynamic and kinetic aspects of fat crystallization was published recently [1]. It is well known that TAGs may crystallize in the α (hexagonal, less stable), β' (orthorhombic), or β (triclinic, most stable) form; the nomenclature scheme following Larsson [2] as reviewed in Hagemann [3], Hernqvist [4], Wesdorp [5], Sato [6], and Ghotra [7]. Each of these polymorphic forms consists of layers in which the molecules have a tuning fork conformation but the orientation of the tuning forks within the layers, as well as the packing of the layers is different. This polymorphic behaviour of TAGs strongly determines the physical properties of the fats. The monoacid saturated TAGs (the three acyl chains are identical) are the simplest in the TAGs family. Because of the simplicity of their structure

*Corresponding author. Tel.: +31 30 253 3125; fax: +31 253 2403.
E-mail address: J.P.J.M.vanderEerden@phys.uu.nl (J.P.J.M. van der Eerden).

0022-0248/$ - see front matter © 2007 Elsevier B.V. All rights reserved.
doi:10.1016/j.jcrysgro.2007.05.048

this group has been examined in more detail than other groups. The three basic α, β' and β polymorphic forms are found [3]. Generally, the polymorphic behaviour of TAGs with an even carbon number n are well represented by the behaviour of tripalmitin (PPP, $n = 16$) and tristearin (SSS, $n = 18$) [3,8–13]. The crystallization and the phase transformation properties of these two triglycerides were found to be very similar. They only differ with respect to the rate at which these processes occur. Both TAGs exhibit a preferential tendency for β-crystallization. The β'-form can only be crystallized from the isotropic melt within a narrow temperature range and shows the typical β'-wide-angle diffraction pattern [13].

Binary mixtures of TAGs show far more complex polymorphic behaviour as compared to pure TAGs. For binary TAG mixtures, the primary factors determining phase behaviour are differences in chain length, the degree of saturation and position of the fatty acid moieties, and the crystal forms. Different phase behaviour is frequently observed for different polymorphs. For example in the mixture PPP–SSS the triglycerides are completely miscible in the less stable phases (α and β') but they form a eutectic system in the stable β-form [14,15]. The same behaviour was observed by Takeuchi et al. [16] for the mixture trilaurin (LLL, $n = 12$)/trimyrisrtin (MMM, $n = 14$), where the carbon numbers in the fatty acid chains differ by 2. When the difference in the carbon chain length differs by 4 or 6 like in the mixtures LLL–PPP and LLL–SSS, the metastable phases (α and β') turn out to be immiscible. Eutectic and monotectic behaviour is observed in the β-form for the LLL–PPP and LLL–SSS systems, respectively, with the α form of SSS co-existing with the β form of LLL under certain conditions [16].

In monolayers at a hydrophilic–hydrophobic interface, e.g. water/oil, water/air or mica/air triglyceride molecules adopt a trident conformation (all hydrocarbon chains pointing into the same direction). In the trident conformation the hydrophilic glycerol group is in contact with the water or the mica surface, and the hydrophobic chains point into the air or the oil [17–22].

In previous work we investigated monolayers of tristearin (SSS, $n = 18$), tripalmitin (PPP, $n = 16$) and triarachidin (AAA, $n = 20$ C), at the air–water interface (Langmuir film) and on a mica surface (Langmuir–Blodgett film). We established the relation between their molecular structure and their monolayer stability. We found that the trident monolayer is the less mobile and the crystal phase is the more stable the longer the acyl chains are. Using AFM the thickness of the trident monolayers was measured. It is 1.49 nm for PPP, 1.75 nm for SSS and 2.2 nm for AAA, corresponding to tilt angles of the molecules of 46°, 49° and 59°, respectively [23].

The aim of this paper is to understand the phase behaviour of binary mixed TAGs: PPP–SSS, PPP–AAA and SSS–AAA at the air–water interface (Langmuir film) and on a mica surface (Langmuir–Blodgett film). We measured the π–A (spreading pressure π vs area per molecule A) diagram of Langmuir films. Starting with a Langmuir film at very small π, where the film is in a low-density "gas" phase, we compressed the film, at a constant rate, to the desired pressure π (forced compression). The Langmuir film was transferred to mica directly after forced compression ($t = 0$) and investigated with AFM immediately.

2. Materials and methods

2.1. Chemicals

Film material: In our experiments we used saturated monoacid triglycerides (their three acyl chains are the same). Tripalmitin (1,2,3-Propanetriyl trihexadecanoate: PPP), Tristearin (1,2,3-trioctadecanoylglycerol: SSS) and Triarachidin (trieicosonoin: AAA) were purchased from Larodan (Sweden) with a stated purity of >99 mass %. Stock solutions of PPP, SSS and AAA with concentration of 1 mM in distilled chloroform were prepared. The stock solutions were mixed in ratios: PPP–SSS (1:1), PPP–AAA (1:1) and SSS–AAA (1:1, 1:3, 3:1).

Subphase: Distilled water was used as a subphase in our Langmuir system for all experiments. The resistivity of the water was 15 MΩ cm.

Substrates: All monolayers were transferred onto freshly cleaved mica.

2.2. Langmuir method

Compression isotherms were measured on a commercial, fully automated Langmuir–Blodgett Trough (model: 311D, Nima Technology Ltd., England). The instrument was equipped with a Teflon trough (283.0 cm^2) and one Delrin barrier. The spreading pressure π was measured with an accuracy of about 0.1 mN/m. The film material was initially spread on the water subphase, dropping 30 μL of 1 mM stock solution dissolved in chloroform, using a 100 μL Hamilton syringe. The conditions were chosen such that initially the average area A per molecule is $A \sim 110$ Å^2. We started (asymmetric) film compression 2 min after spreading. In the experiments described here we used the *forced compression* operation mode, where the position of the barrier, and hence the trough length $l(t)$ ahead of the barrier, is given. Then the resulting spreading pressure $\pi(t)$ is registered. In this mode we chose barrier velocities of the order of 1 cm/min, which according to the literature should be slow enough that the Langmuir film stays close to thermodynamic equilibrium. It should be mentioned however, that in previous work [23] we have shown that, for condensed phases this compression rate is still too high for the film to be in equilibrium.

2.3. Langmuir–Blodgett film transfer

In order to obtain LB films, first a substrate was immersed perpendicularly in the aqueous subphase. We started with a very small initial surface pressure ($\pi = 0$ mN/m), and compressed the monolayer slowly (1 cm/min) to the

final pressure. To obtain a LB film that is characteristic for forced compression, the film was transferred immediately by vertical pulling of the substrate through the air–water interface at a speed of 2 mm/min. During the transfer the surface pressure was kept constant by appropriately moving the barrier. The transfer process takes a few minutes. After deposition the LB-films were dried in air and kept in closed containers until use. All experiments were done at $20 \pm 1\,^{\circ}C$.

2.4. AFM measurements

The samples were examined with AFM immediately after preparation. Imaging was done with a Nanoscope (R) IIIa (Digital Instruments, Santa Barbara, CA) in contact mode with oxide-sharpened silicon nitride tip ($k = 0.06$ N/m). The AFM was equipped with a J scanner ($176 \times 176\,\mu m$; z limit $= 5.349\,\mu m$). All images were processed using procedures for flattening in Nanoscope III software version 5.12r5 without any filtering. To check if the monolayer is successfully transferred to the mica surface we measured at least five different spots (each $150\,\mu m^2$) of every sample.

3. Langmuir observations

In previous work [23] we already discussed the shape of the typical $\pi-A$ isotherms of PPP, SSS and AAA, where two different regimes can be recognized for the three triglycerides. The *condensation area* A_{cond} and *condensation pressure* π_{cond} have been described as values indicating the transfer from "gaseous" to "condensed" phase. The *collapse pressure* π_{col} is the surface pressure at which the monolayer collapses to form multilayer structures. For the studied triglycerides π_{col} was about 40–48 mN/m and increased with decreasing chain length: $\pi_{col}(AAA) < \pi_{col}(SSS) < \pi_{col}(PPP)$. With our LB instrument the *collapse pressure* π_{col} was difficult to reach because of details in its construction. For the mixtures we measured similar $\pi-A$ isotherms as for the single components (Fig. 1). The measured $\pi-A$ data for the mixtures showed that the pressure range, where the transition from one regime to another takes place, was rather wide. For the mixtures the adsorption isotherm was always between the isotherms of the single components. An exception was the mixture SSS–AAA, for which the $\pi-A$ isotherm almost coincided with the isotherm of AAA for $\pi < 15$ mN/m. In order to get reliable and unbiased estimations for A_{cond} and π_{cond}, we fitted the isotherms with:

$$\pi(A) \approx \frac{2\pi_{cond}}{a} h(A - A_{cond}, a), \tag{1}$$

where A_{cond}, a and π_{cond} are fitting parameters. The function

$$h(x,a) \equiv \frac{1}{2}\left(\sqrt{x^2 + a^2} - x\right) \tag{2}$$

is a hyperbola interpolating between the asymptotes $h(x, a) \approx |x|$ for large negative x and $h(x, a) \approx 0$ for large positive x. The asymptotes intersect at $h = a/2$ for $x = 0$. Fitting a number of isotherms (15) that were obtained at compression velocity 1 cm/min we found $A_{cond} = 64 \pm 1$ Å^2 and $\pi_{cond} = 9 \pm 3$ mN/m for SSS–AAA; $A_{cond} = 63 \pm 1$ Å^2 and $\pi_{cond} = 10 \pm 3$ mN/m for PPP–SSS and $A_{cond} = 63 \pm 3$ Å^2 and $\pi_{cond} = 11 \pm 2$ mN/m for PPP–AAA. Together with the corresponding data for the pure PPP, SSS and AAA systems, these results are presented in Fig. 2.

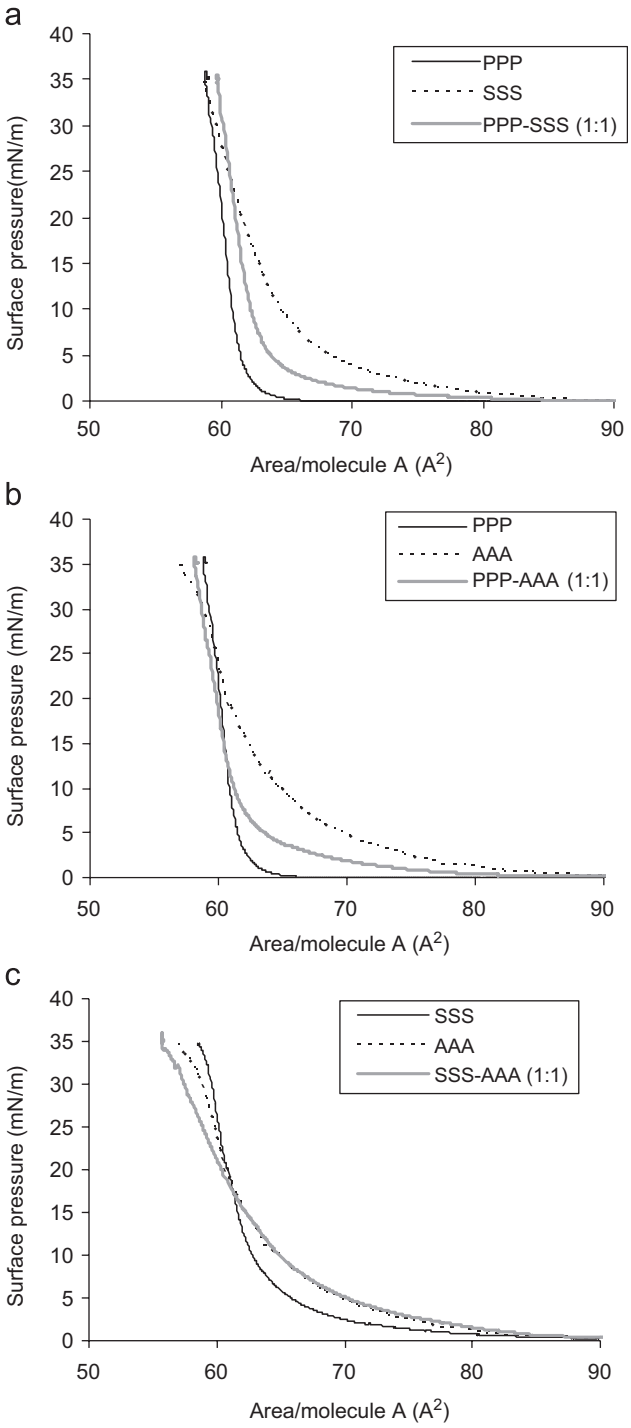

Fig. 1. Surface pressure vs area isotherms of tripalmitin (PPP), tristearin (SSS) and triarachidin (AAA) and their mixtures at air–water interface, at 20 °C, obtained by forced compression at a rate of 1 cm/min.

The fact that A_{cond} is around 63 Å^2 for all studied triglycerides and their mixtures is consistent with a trident conformation of triglyceride molecules in a monolayer film at the air–water interface. Indeed, the cross-sectional area per hydrocarbon chain for tristearin at 20 °C in the α phase (the α phase has the most mobile acyl chains) is 19.7 Å^2 [24]. Our isotherms are consistent with earlier reports [17,21].

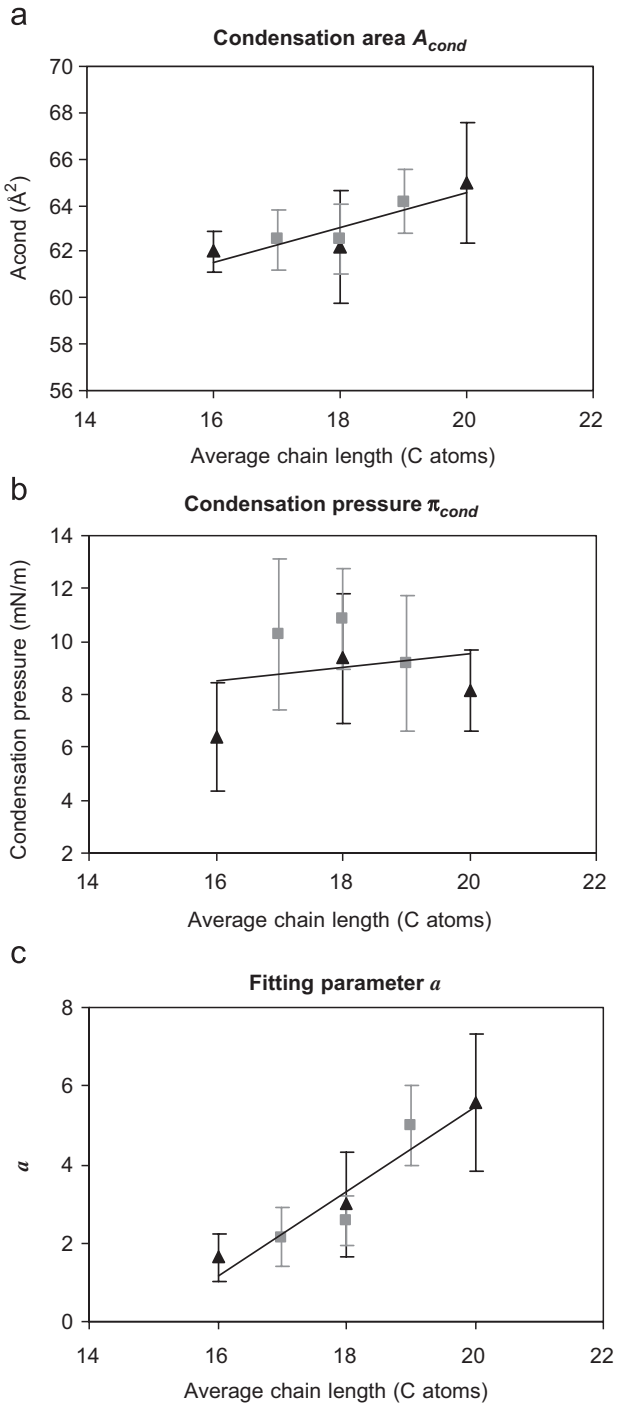

Fig. 2. A_{cond} (a), π_{cond} (b) and fitting parameter a (c) for triglycerides (▲) and their mixtures (■). X-axis presents the number of the carbon atoms in the triglyceride chains: PPP (16), SSS (18) and AAA (20). For the mixtures it was calculated as follow: 17 = PPP–SSS (1:1), 18 = PPP–AAA (1:1) and 19 = SSS–AAA (1:1).

The fact that π_{cond} is almost the same for the investigated pure triglycerides and their mixtures as well (8–10 mN/m), is consistent with the idea that the packing properties of the hydrocarbon chains is mainly determined by short range repulsive interactions. The effective repulsion is quite independent of the chain length and compositions, which shows that mixing of triglycerides does not change their packing properties drastically. The tendency of A_{cond} and π_{cond} to increase slightly with increasing chain length reflects a slightly enhanced repulsion of longer chains.

The value of the fitting parameter a (Eq. (1)) describes the sharpness of the gas-condensed transition and is found to depend strongly on the chain length (the smaller a, the sharper is the transition). This is also seen in Fig. 1 where the $\pi-A$ isotherm for PPP is sharper than those for SSS and AAA. This observation can be understood if one realizes that the shorter PPP molecules are stiffer than the longer SSS and AAA. The longer chains will spread somewhat more in lateral direction. The isotherms in Fig. 1 suggest that in a moderately dense packed monolayer at the air–water interface the longer triglycerides interact already at significantly larger intermolecular distances than the shorter ones. The fitting parameter a is rapidly increasing with increasing chain length. Apparently the presence of PPP in a mixture reduces the hindering of the motion of the longer molecules and thus sharpens the transition from the gas to the condensed phase.

In general the $\pi-A$ isotherms of the mixtures interpolate linearly between the isotherms of the pure components. For example, the isotherm of the PPP–AAA mixture (average chain length 18) is very similar to the isotherm of pure SSS (chain length 18). Thus from the $\pi-A$ isotherms alone one would be tempted to conclude that the triglycerides mix (almost) ideally. In the remainder of this paper, we show that this conclusion is incorrect. We investigated Langmuir–Blodgett monolayers of the mixtures with AFM. Our experimental results clearly show non-ideal behaviour, and even phase separation.

4. AFM observations

To investigate the structure of the three mixtures we withdrew Langmuir monolayers immediately after forced compression to $\pi = 20$ mN/m. We chose this surface pressure because is in the middle of the condensed region of the $\pi-A$ isotherms. We know from the $\pi-A$ isotherms that it is well above the condensation pressure π_{cond}, but still below the collapse pressure π_{col}.

4.1. PPP–SSS structure

The AFM images of PPP–SSS (1:1) showed a homogeneous monolayer with thickness 1.6 ± 0.1 nm, i.e. somewhere between the measured thicknesses of PPP and SSS

(Figs. 3a and d). The mixed monolayer contains more holes than monolayers of pure systems, which are almost defect free. This is the first indication that due to the difference in the chain length of the two components in the mixture, random packing of longer and shorter molecules is thermodynamically not optimal. In some regions of the samples shallow depressions are observed that may be the onset of phase separation (Figs. 3b and c). It was difficult to measure their depth with AFM. We estimated a height difference of 0.2 ± 0.1 nm (Figs. 3c and f). The carbon chain length of PPP and SSS differs by 2 carbon atoms, which is ~0.25 nm [25]. The thickness of the monolayers, which we obtained by extrapolation to zero scanning force, is $d_0 = 1.49$ nm for PPP, $d_0 = 1.75$ nm for SSS and $d_0 = 2.19$ nm for AAA. These monolayer thicknesses correspond to tilt angles of the molecules of 46°, 49° and 59°, respectively [23]. The measured height difference of 0.2 ± 0.1 nm in the mixture PPP–SSS (1:1) is close to the expected height difference of ~0.3 nm between tilted PPP and SSS monolayers. The fact that most of the AFM images of PPP–SSS (1:1) showed a homogeneous monolayer supports the idea that PPP and SSS have only a weak tendency to phase separate.

In Ref. [23] we demonstrated that the apparent thickness depends strongly on the AFM scanning force. Even relatively small scanning forces compress triglyceride

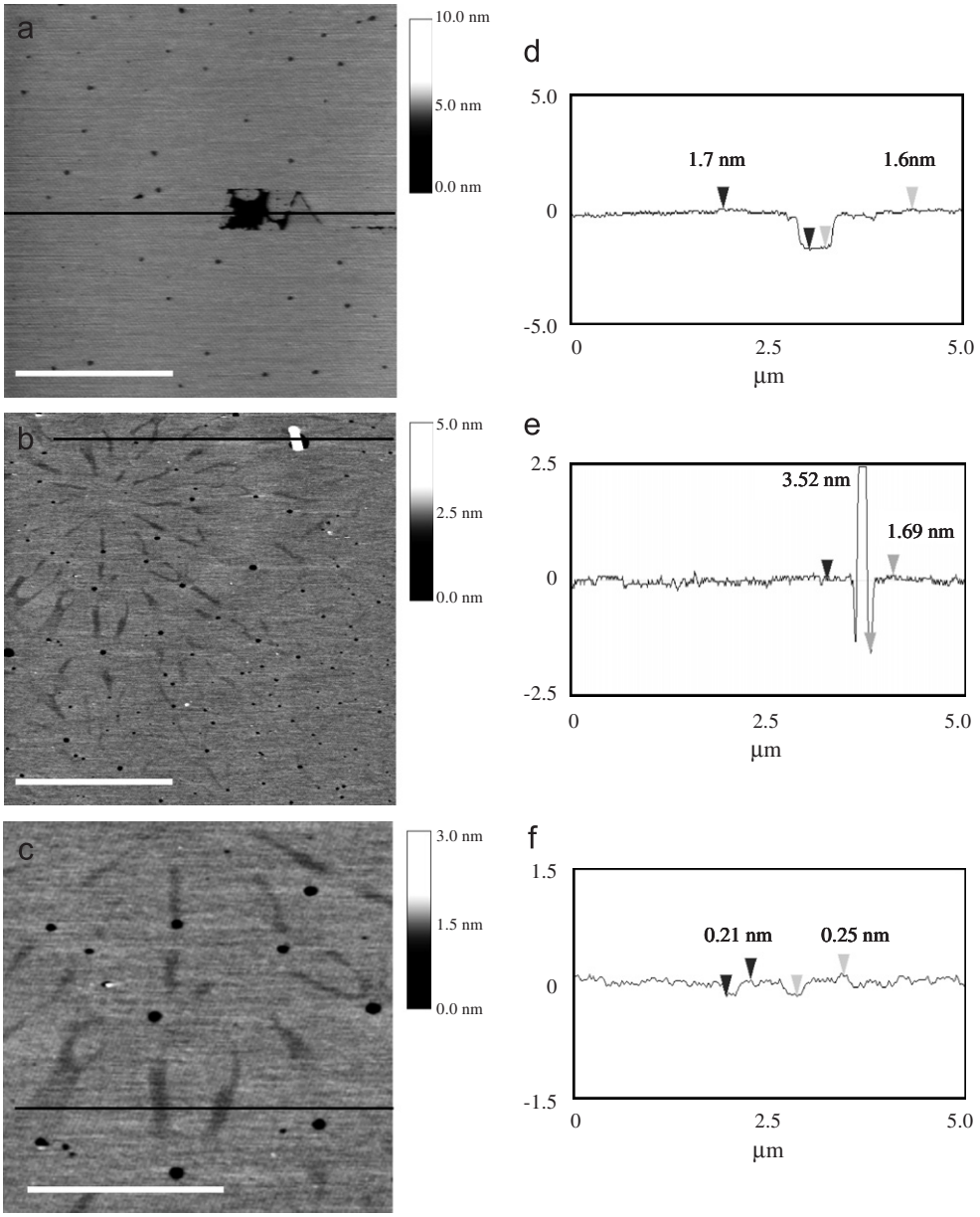

Fig. 3. (a) AFM height image of PPP–SSS monolayer transferred immediately after forced compression to $\pi = 20$ mN/m. The black square is a hole in the monolayer produced by scanning at a high AFM force (F~30 nN). The monolayer is scanned at AFM force F~1 nN. (b) Another area of the same sample, where the onset of phase separation was observed. (c) Zoomed image of (b). The corresponding cross sections are given in (d–f). The scale bar is 2 µm for (a and b) and 1 µm for (c). Height differences are given by the numbers at the markers.

monolayers. We showed that the compressibility varies little between the investigated pure triglycerides. To measure the real monolayer thickness d_0 of the mixture PPP–SSS (1:1) we used the same procedure as in Ref. [23]. By scanning with a relatively large force $F \approx 30\,\mathrm{nN}$ we scratched a rectangular hole in the monolayer with the AFM tip. Then a larger area, including the hole, was scanned with small forces $F = 1$–$8\,\mathrm{nN}$ (Fig. 4). The height difference between the hole and the surrounding film gives an apparent thickness d' for each strength of the scanning force F. We investigated three different holes in one sample (Fig. 4).

In Fig. 4 we see that the dependence of d' on the scanning force F for the mixtures of triglycerides and for the pure systems is very similar. By definition the isothermal compressibility of three dimensional materials is

$$K_T = -\frac{1}{V}\left(\frac{\partial V}{\partial P}\right)_T. \tag{3}$$

Analogously the uniaxial (vertical) isothermal film compressibility can be defined as

$$K_{film} = -\frac{1}{d'}\left(\frac{\partial d'}{\partial P_\perp}\right)_T \approx \frac{1}{3}K_T, \tag{4}$$

where the last approximation is valid if the elastic properties of the film are isotropic and the same as of the bulk material. In our system we measure the AFM force F. The vertical pressure in this case would be

$$P_\perp = F/area, \tag{5}$$

where *area* is the area that is effectively depressed by the tip. Unfortunately we cannot accurately estimate *area*. For practical reasons we define the quantity $\tilde{K}$ as

$$\tilde{K} \equiv -\frac{1}{d'}\frac{\partial d'}{\partial F} \approx \frac{1}{3}\frac{K_T}{\mathrm{area}}. \tag{6}$$

The approximate equality is obtained using Eqs. (4) and (6). Somewhat loosely, we shall refer to $\tilde{K}$ as *film compressibility* from now on.

The film compressibility of the monolayer, given by the slope of $d'(F)$ curves, is slightly higher for PPP–SSS (1:1) ($\tilde{K} = 0.08 \pm 0.01\,\mathrm{nN}^{-1}$) than for pure PPP and SSS ($\tilde{K} = 0.07 \pm 0.01\,\mathrm{nN}^{-1}$). Note the value of $\tilde{K}$ is remarkably reproducible and hardly depends on the tip used. In view of Eq. (5) this means that the contact area is mainly determined by the film, and little influenced by the precise tip shape. Comparing our $\tilde{K}$ values with a typical value $K_T \approx 2 \times 10^{-8}\,\mathrm{m^2/N}$ for soft materials we see that *area* is of the order of $100\,\mathrm{nm}^2$, which is much larger than direct tip-film contact area.

The real thickness d_0, corresponding to scanning force $F = 0$ is presented in Fig. 5. As shown in Fig. 5 for PPP–SSS (1:1) we found two distinct results, $d_0 = 1.50 \pm 0.02\,\mathrm{nm}$ and $d_0 = 1.69 \pm 0.01\,\mathrm{nm}$. These values are close to $d_0(\mathrm{PPP}) = 1.49 \pm 0.02\,\mathrm{nm}$ and $d_0(\mathrm{SSS}) = 1.75 \pm 0.02\,\mathrm{nm}$, respectively, and we suppose that they are the thickness of PPP- and SSS-rich areas in the monolayer, respectively.

We conclude that in the mixture PPP–SSS (1:1) incomplete phase separation takes place. The PPP-rich regions contain dissolved SSS molecules and SSS-rich regions contain dissolved PPP molecules. The dissolved molecules influence the average thickness of the monolayer. We cannot completely exclude the possibility that PPP and SSS are completely separated in very small domains that cannot be detected by the AFM.

Like in monocomponent systems [22,23] we found higher domains on top of the PPP–SSS monolayer. Most of them had a thickness of $3.5 \pm 0.1\,\mathrm{nm}$ (Figs. 3b and e). This corresponds to molecules of PPP or SSS in tuning fork conformation. Similar domains are formed when a Langmuir monolayer of the single component is transferred immediately at $\pi = 20\,\mathrm{mN/m}$ ($3.3 \pm 0.1\,\mathrm{nm}$ for PPP and $3.5 \pm 0.1\,\mathrm{nm}$ for SSS) [23]. The composition of the crystals on top of the PPP–SSS monolayer is not clear. They could contain either PPP or SSS or both types of molecules.

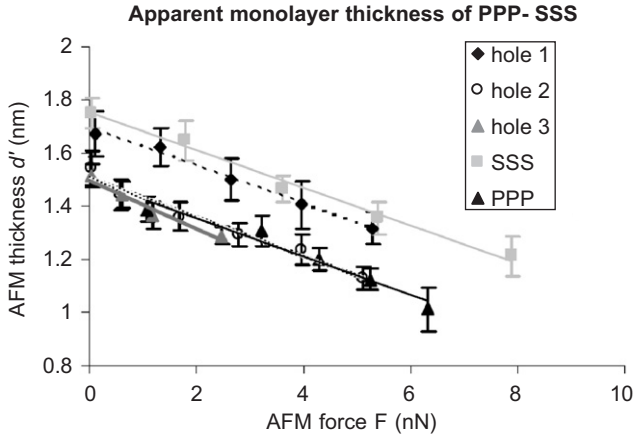

Fig. 4. Measured layer thickness d' for PPP, SSS and PPP–SSS (1:1) as a function of applied AFM force F at surface pressure $\pi = 20\,\mathrm{mN/m}$.

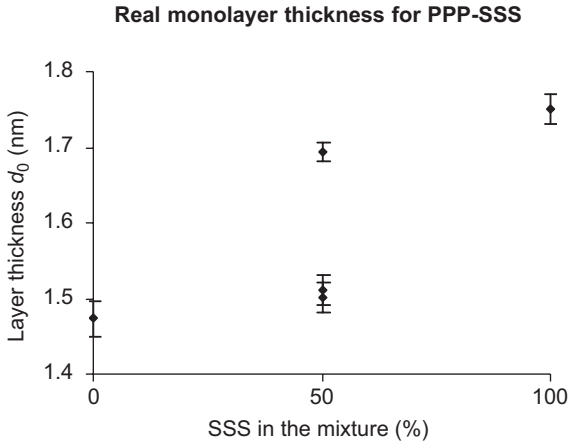

Fig. 5. Real monolayer thickness d_0 for PPP, SSS and PPP–SSS (1:1) for three different holes at surface pressure $\pi = 20\,\mathrm{mN/m}$. The d_0 values are found by extrapolation of the apparent monolayer thickness d' in Fig. 4 to AFM force $F = 0\,\mathrm{nN}$.

4.2. SSS–AAA structure

The AFM images of SSS–AAA (1:1) showed a homogeneous monolayer (Fig. 6). To measure the thickness of the monolayer we used the same procedure as described in Section 4.1. In order to get reliable and unbiased estimations for d_0 this procedure was repeated for three independent holes in one sample (Fig. 7). For SSS–AAA (1:1) we found $d_0 = 1.95 \pm 0.02$ nm by extrapolation of the apparent monolayer thickness d' in Fig. 7 to AFM force $F = 0$ nN. The film compressibility of the mixture monolayer $\tilde{K} = 0.08 \pm 0.01\,\mathrm{nN}^{-1}$ was very close to that of the pure monolayers ($\tilde{K} = 0.07 \pm 0.01\,\mathrm{nN}^{-1}$). We did not observe any crystals on top of the monolayer. Contrary to PPP–SSS we saw no indications for phase separation. No domains were observed. This suggests the absence Of phase separation in SSS–AAA. To investigate this further we also studied (1:3) and (3:1) mixtures of SSS–AAA. The same absence of domains was observed for 1:3 and 3:1 mixtures (data not shown). The monolayer thickness d_0 depended linear on composition (Fig. 8). The film compressibility was the same for all SSS–AAA mixtures.

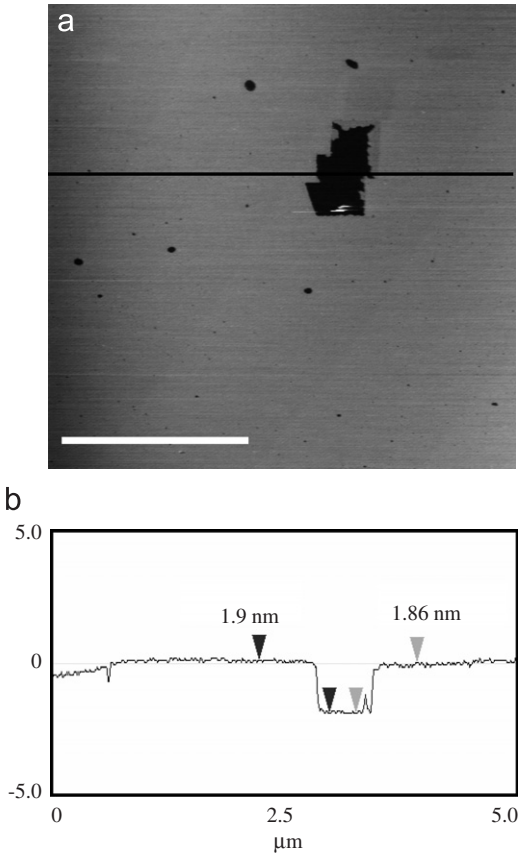

Fig. 6. (a) AFM height image of SSS–AAA (1:1) monolayer transferred immediately after forced compression to $\pi = 20$ mN/m and the corresponding cross section in (b). The black square is a hole in the monolayer produced by scanning at a high AFM force ($F \sim 30$ nN). The monolayer is scanned at AFM force $F \sim 1$ nN. The scale bar is 2 μm and the vertical scale is 10 nm. Height differences are given by the numbers at the markers.

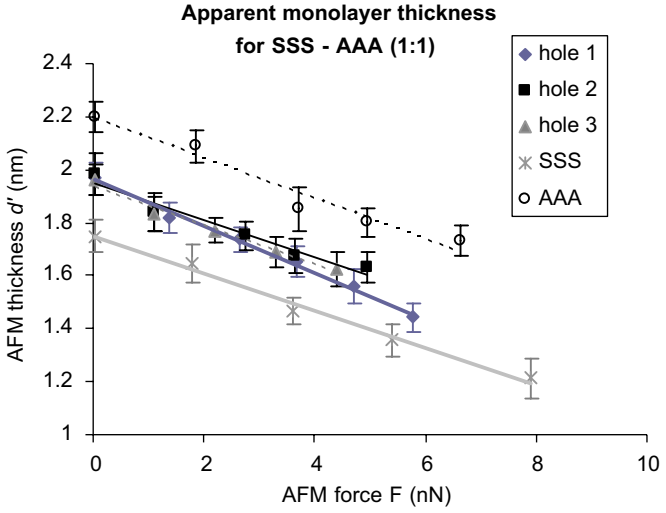

Fig. 7. Measured layer thickness d' for SSS, AAA and SSS–AAA (1:1) as a function of applied AFM force F at surface pressure $\pi = 20$ mN/m.

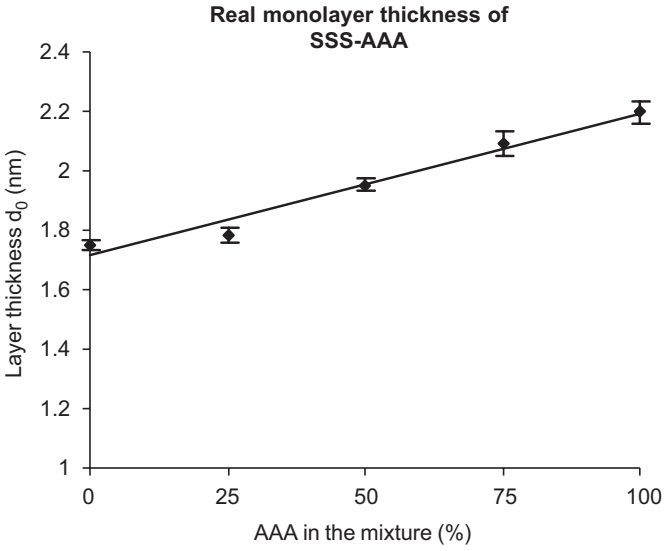

Fig. 8. Real monolayer thickness d_0 for SSS–AAA at surface pressure $\pi = 20$ mN/m as a function of the mole fraction of AAA in the mixture. The values are found by extrapolation of the apparent monolayer thickness d' to AFM force $F = 0$ nN.

All these observations support that SSS–AAA forms (almost) ideal mixtures.

4.3. PPP–AAA structure

In some cases AFM images of LB-films of PPP–AAA (1:1) show areas where phase separation is hardly visible (Figs. 9a–c) as in the PPP–SSS (1:1) mixture. There are other areas however, with very well separated domains (Figs. 9d–f). To measure monolayer thicknesses for different domains, we used the same procedure as described in Section 4.1. We measure the monolayer thickness in different areas independently. As before we corrected

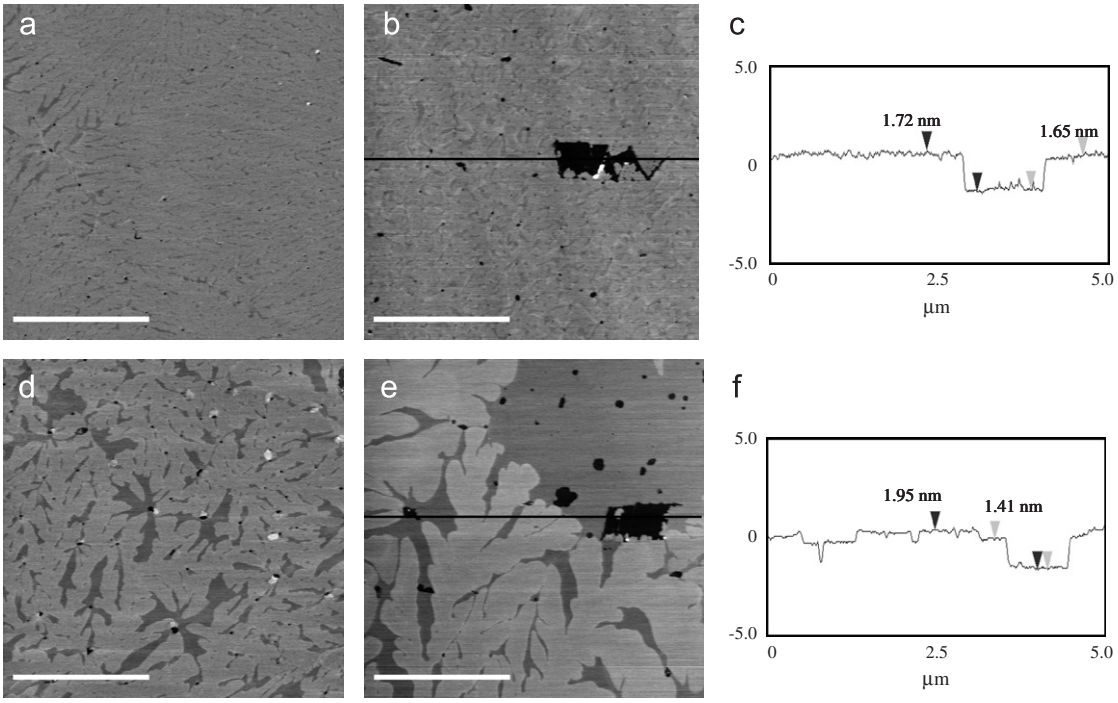

Fig. 9. (a and b) AFM height images of PPP–AAA (1:1) monolayer transferred immediately after forced compression to $\pi = 20\,\mathrm{mN/m}$ with little indication of phase separation. The corresponding cross section is given in (c). (d and e) Areas of the same sample, where phase separation is clearly visible. The corresponding cross section is given in (f). Black squares are holes in the monolayer produced by scanning at a high AFM force (F~30 nN). The monolayers are imaged at AFM force F~1 nN. The scale bar is 2 μm and the vertical scale is 10 nm for all images. Height differences are given by the numbers at the markers.

for the compression of the AFM at low scanning force (Fig. 10).

The thickness of the PPP–AAA (1:1) monolayer, at positions where the phase separation is not obvious, is $d_0 = 1.86 \pm 0.05$ nm, i.e. between the monolayer thicknesses of the single components. The film compressibility $\tilde{K} = 0.11 \pm 0.02\,\mathrm{nN}^{-1}$ at such positions is larger than for PPP and AAA separately ($\tilde{K} = 0.07 \pm 0.01\,\mathrm{nN}^{-1}$).

At positions with clear phase separation the two different domains had thicknesses $d_0 = 1.42 \pm 0.01$ nm and $d_0 = 1.96 \pm 0.03$ nm. These heights are close to the height of PPP ($d_0 = 1.49 \pm 0.02$ nm) and AAA ($d_0 = 2.19 \pm 0.04$ nm) monolayers, respectively [23]. The thickness of the higher domains is somewhat less than the thickness of pure AAA. We assume that in regions like those in Figs. 9d and e the higher domains are AAA-rich. The film compressibility of AAA-rich areas $\tilde{K} = 0.10 \pm 0.01\,\mathrm{nN}^{-1}$ is higher than the one of the pure AAA ($\tilde{K} = 0.07 \pm 0.01\,\mathrm{nN}^{-1}$). This is consistent with the hypothesis that the AAA-rich domains contain some PPP molecules, which lower the packing density of AAA molecules and thus make the monolayer more compressible. The lower domains are similar in thickness and have the same film compressibility as pure PPP monolayers ($\tilde{K} = 0.07 \pm 0.01\,\mathrm{nN}^{-1}$). We assume that they are PPP-rich. The fact that in the phase separated regions the AAA-rich domains occupy a significantly larger

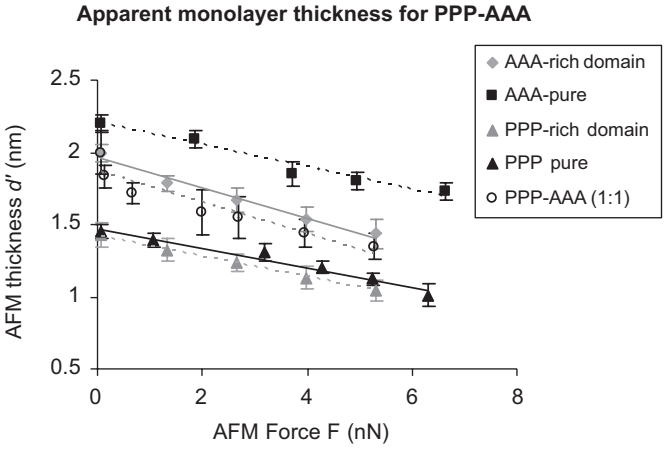

Fig. 10. Measured layer thickness d' for PPP, AAA from the monolayers of the pure components and in the mixture PPP–AAA (1:1) as a function of applied AFM force F at surface pressure $\pi = 20\,\mathrm{mN/m}$.

fraction of the surface area than the PPP-rich domains (Fig. 9) indicates that PPP is more soluble in AAA than AAA in PPP. Moreover, the fact that the lower, PPP-rich, domains are similar in thickness to pure PPP monolayers suggests that AAA is hardly soluble in PPP. Such a tendency is reasonable, since it will be energetically more unfavourable to dissolve long molecules in a thin layer than

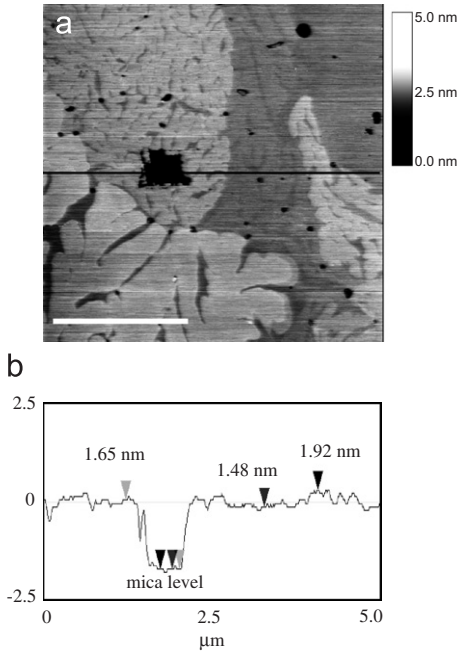

Fig. 11. (a) AFM height image of PPP–AAA (1:1) monolayer transferred immediately after forced compression to $\pi = 20\,\mathrm{mN/m}$. The corresponding cross section in (b) presents three different domains in the mixture. The black square is a hole in the monolayer produced by scanning at a high AFM force ($F \sim 30\,\mathrm{nN}$). The monolayer is scanned at AFM force $F \sim 1\,\mathrm{nN}$. The scale bar is 2 μm. Height differences are given by the numbers at the markers.

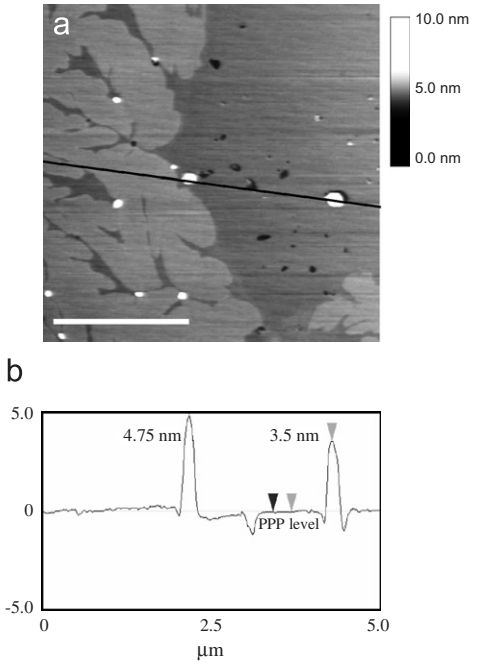

Fig. 12. AFM height image of PPP–AAA (1:1) monolayer transferred immediately after forced compression to $\pi = 20\,\mathrm{mN/m}$ (a) and the corresponding cross section in (b). The image presents crystals on top of the monolayer. Their height is measured from the PPP level. The scale bar is 2 μm. Height differences are given by the numbers at the markers.

reverse. In some of the AFM images of PPP–AAA (1:1) monolayer we observed three different levels (Fig. 11). The highest and lowest levels corresponded to the thickness of AAA-rich and PPP-rich layers, respectively. The area at the middle level was very irregular, showing the onset of phase separation as for PPP–SSS in Fig. 3. Its thickness of about 1.65 nm corresponds to the thickness of PPP–AAA monolayers before demixing, see Figs. 9a–c.

On top of the PPP–AAA (1:1) monolayer we observed crystals with thicknesses varying from 3.5 to 4.7 nm (Fig. 12). These values coincide with the measured values for PPP crystals on top of monolayer in α- and β-like phases. We also know that PPP crystallizes faster from a monolayer than the longer AAA [23]. In view of these facts we suppose that the crystals, formed on top of PPP–AAA monolayer, are (almost) pure PPP. This conclusion however, cannot be drawn with certainty from the present AFM observation alone.

5. Discussion and conclusions

In this study we have obtained AFM images that reveal the structure of binary mixed TAG films (PPP–SSS, PPP–AAA and SSS–AAA), formed at air–water interfaces. Based on Langmuir and AFM experiments we established the relation between their phase behaviour and the chain length of the two components. We compared the results with those for the pure components.

It is known from the literature that the phase behaviour in binary mixed TAGs in 3D crystal structure strongly depends on the difference between the TAGs chain length [14–16]. When the number of carbon atoms in the alkyl chains differs by 2, the mixtures are complete miscible in the less stable forms (α and β′) and they form a eutectic system for the β-form. When the difference in the carbon chain length is 4 or 6 also the metastable phases (α and β′) are immiscible. Eutectic and monotectic behaviour is observed in the β-form for the LLL–PPP and LLL–SSS systems, respectively. The α-form of SSS may co-exist with the β-form of LLL under certain conditions [17].

In our 2D systems of binary mixed TAGs we have found a similar dependence on the difference between the TAGs chain length. In order to compare quantitatively the condensation area A_{cond}, the condensation pressure π_{cond} and the isotherm sharpness a, Langmuir isotherms were fitted for all mixtures and single components. At the air–water interface the binary mixed TAGs form trident monolayers, like the single components. This is confirmed by the Langmuir adsorption isotherms, which show that $A_{\mathrm{cond}} = 63 \pm 2\,\mathrm{Å}^2$ and $\pi_{\mathrm{cond}} = 8$–$10\,\mathrm{mN/m}$ are very similar for all systems (see Section 3).

The value of the fitting parameter a, which characterizes the sharpness of the transition from "gas" to "condensed" phase in the $\pi - A$ isotherm, varied considerably for different systems. In the mixtures a was larger for SSS–AAA, than for PPP–SSS and PPP–AAA. In the single components $a(\mathrm{PPP}) < a(\mathrm{SSS}) < a(\mathrm{AAA})$. We found

a linear increase of a with average chain length for all systems (Fig. 2c). Based on our results we conclude that smaller molecules have a higher mobility in the film and make the transition from one phase to another sharper. This was clear for the single component films and for all mixtures. Judging on Langmuir data alone, one could be tempted to conclude that PPP, SSS and AAA are well miscible in the monolayer regime. Our AFM analysis however, shows that this conclusion would be incorrect. AFM thus is shown to be essential for a sound interpretation of monolayer data.

From the AFM images of LB-films of PPP–SSS, SSS–AAA and PPP–AAA, withdrawn at $\pi = 20\,\mathrm{mN/m}$ it is seen that the mica substrate is covered by a monolayer. Apparently the Langmuir monolayer can be successfully transferred from the water surface in the Langmuir trough to a mica surface to form a Langmuir–Blodgett film there.

The AFM images of LB-monolayers transferred immediately after forced compression at $\pi = 20\,\mathrm{mN/m}$ for PPP–SSS (1:1) showed a monolayer, which in some regions was quite homogeneous. In other regions of the same sample the onset of phase separation was observed. In the regions with the onset of phase separation two different layer thicknesses were found. The estimated height difference ($0.2 \pm 0.1\,\mathrm{nm}$) corresponds to the length of a two carbon atom chain at a tilt angle of about 50° (0.2 nm). The thickness of the monolayer d_0, measured from the homogeneous areas of the sample varied from 1.5 to 1.7 nm (Fig. 5).

We concluded that in the mixture PPP–SSS (1:1) incomplete phase separation takes place, the difference in composition of the PPP-rich and SSS-rich phases is relatively small. The alternative hypothesis, that the phase separation is complete, but PPP and SSS form too small domains to be detected by AFM, seems unlikely but cannot be excluded with certainty.

The mixture SSS–AAA, where the difference in the carbon chain length is two atoms as well behaved different from PPP–SSS (1:1). All AFM images of SSS–AAA (1:1, 1:3 and 3:1), transferred immediately after forced compression to surface pressure $\pi = 20\,\mathrm{mN/m}$, showed homogeneous monolayers. We never observed the onset of phase separation. The monolayer thickness d_0 varied linearly with composition between the monolayer thicknesses of the single components (Fig. 8). Based on these observations we concluded that SSS and AAA mix (almost) ideally. Due to stronger interactions between longer alkyl chains, the sensitivity for differences in the chain length decreases with increasing alkyl chain length.

In the mixture PPP–AAA (1:1) (four carbon atoms difference) phase separation was observed. From the AFM images it is seen that there were regions, where only the onset of phase separation was clearly visible and regions, where it was well defined (Fig. 9). The measured height difference between the higher and the lower domains was $0.6 \pm 0.1\,\mathrm{nm}$. This difference is close to the difference in monolayer thickness of the single components PPP and AAA with $d_0 = 1.49$ and 2.19 nm, respectively. We assume that the highest domains in the mixture correspond to AAA-rich and the lowest to PPP-rich phases. Precise measurement of the thickness of the different domains in the mixture as a function of the AFM force showed that the thickness of the higher domains is somewhat smaller than the thickness of pure AAA monolayers. The film compressibility of the higher domains is slightly larger than for pure AAA monolayers. The thickness of the lower domains was close to the thickness of a PPP monolayer (Fig. 10). The area occupied by higher domains in PPP–AAA (1:1) monolayer was more than 50% of the total area. We concluded that the higher domains in the mixture are not "pure" AAA but are rich in AAA, with a significant fraction of dissolved PPP molecules. Probably the lower domains are PPP with little dissolved AAA. Some AFM images of PPP–AAA (1:1) (Fig. 11) showed even other domains with thicknesses between the highest and lowest measured thickness. These regions may correspond to PPP–AAA systems that are in initial state of phase separation.

Our results for the film compressibility (Fig. 13) showed that the monolayers of the mixtures tend to have a slightly higher compressibility than those of the pure components. We suppose that in the pure systems due to the identity in the chain length the molecules pack better and thus make the monolayer less compressible.

The AFM observations of phase separation in the investigated TAG mixtures support the idea of our previous papers [22,23] that forced compression at ~1 cm/min is probably too fast to stay close to equilibrium.

From Ref. [23] we know that at surface pressure $\pi = 20\,\mathrm{mN/m}$ PPP and SSS form crystals in tuning fork conformation on top of the monolayer. For SSS they are all in β-phase, for PPP, crystals with α- and β-like structures coexist in the LB-film. We also know that the rate of crystallization on top of the monolayer is highest for PPP, lower for SSS and almost zero for AAA.

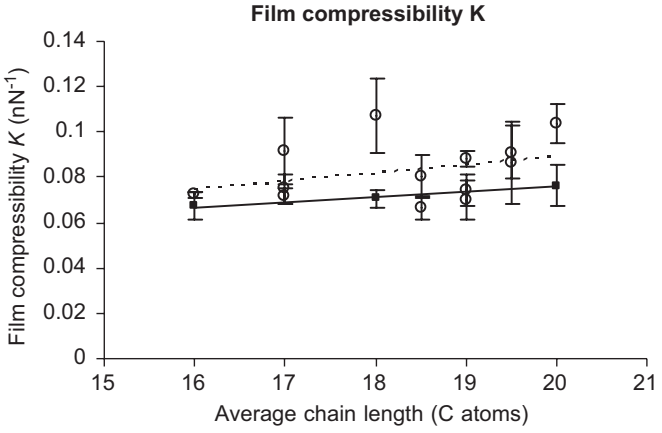

Fig. 13. Film compressibility $\tilde{K}$ as a function of the chain length for the pure components (■) and their mixtures (○).

The AFM images of LB-films, withdrawn at surface pressure $\pi = 20\,\mathrm{mN/m}$ of PPP–SSS and PPP–AAA mixtures often showed small crystals on top of the monolayer. The thickness of these crystals in PPP–SSS and PPP–AAA mixed monolayers varies from 3.5 to 4.7 nm (Figs. 3b, e and 12). These thicknesses correspond to TAG crystals in tuning fork conformation as we also found in LB-films of the pure components. From our data we cannot deduce the crystal composition. On SSS–AAA mixed monolayers, like on AAA, such crystals were not observed.

References

[1] C. Himawan, V.M. Starov, A.G.F. Stapley, Adv. Colloid Interface Sci. 122 (2006) 3.
[2] K. Larsson, Acta Chem. Scand. 20 (1966) 2255.
[3] J.W. Hagemann, in: N. Garti, K. Sato (Eds.), Crystallization and Polymorphism of Fats and Fatty Acids, Marcel Dekker, New York, 1988, p. 9.
[4] L. Hernqvist, in: N. Garti, K. Sato (Eds.), Crystallization and Polymorhism of Fats and Fatty Acids, Marcel Dekker, New York, 1988, p. 97.
[5] L.H. Wesdorp, Liquid-multiple solid phase equilibria in fats, Ph.D. Dissertation, Delft University of Technology, 1990.
[6] K. Sato, Fett-Lipid 101 (1999) 467.
[7] B.S. Ghotra, S.D. Dyal, S.S. Narine, Food Res. Int. 35 (2002) 1015.
[8] K. Sato, T. Kuroda, J. Am. Oil Chem. Soc. 64 (1987) 124.
[9] M. Kellens, W. Meeussen, C. Riekel, H. Reynaers, Chem. Phys. Lipids 52 (1990) 79.
[10] M. Kellens, W. Meeussen, R. Gehrke, H. Reynaers, Chem. Phys. Lipids 58 (1991) 131.
[11] M. Kellens, W. Meeussen, H. Reynaers, J. Am. Oil Chem. Soc. 69 (1992) 906.
[12] A. Desmedt, C. Culot, C. Deroanne, F. Durant, V. Gibon, J. Am. Oil Chem. Soc. 67 (1990) 653.
[13] M. Kellens, W. Meeussen, H. Reynaers, Chem. Phys. Lipids 55 (1990) 163.
[14] E.S. Lutton, J. Am. Chem. Soc. 77 (1955) 2646.
[15] M. Kellens, W. Meeussen, A. Hammersley, H. Reynaers, Chem. Phys. Lipids 58 (1991) 145.
[16] M. Takeuchi, S. Ueno, K. Sato, Cryst. Growth Des. 3 (2003) 369.
[17] T. Bursh, K. Larsson, M. Lundquist, Chem. Phys. Lipids 2 (1968) 102.
[18] J.A. Hamilton, D.M. Small, in: Proc. Nat. Acad. Sci. USA 78 (1981) 6878.
[19] J.A. Hamilton, Biochem. 28 (1989) 2514.
[20] P.M. Claesson, A. Dedinaite, B. Bergenstahl, B. Campbell, H. Christenson, Langmuir 13 (1997) 1682.
[21] M. Michalski, P. Brogueira, A. Goncalves da Silva, B. Saramago, Eur. J. Lipid Sci. Technol. 103 (2001) 677.
[22] A.N. Zdravkova, J.P.J.M. van der Eerden, J. Crystal Growth 293 (2) (2006) 528.
[23] A.N. Zdravkova, J.P.J.M. van der Eerden, Cryst. Growth Design (2006, accepted for publication).
[24] C. Akita, T. Kawaguchi, F. Kaneko, O. Yamamuro, H. Akita, M. Ono, M. Suzuki, J. Crystal Growth 275 (2005) e2187.
[25] S. De Jong, Triacylglycerol crystal structures and fatty acid conformations, a theoretical approach, Ph.D. Thesis, University of Utrecht, The Netherlands, 1980.